

# Dynamic structure factor of one-dimensional Fermi superfluid with spin-orbit coupling

Zheng Gao<sup>1</sup>, Lianyi He<sup>2</sup>, Huaisong Zhao<sup>1,\*</sup>, Shi-Guo Peng<sup>3,†</sup> and Peng Zou<sup>1,‡</sup>

<sup>1</sup>*College of Physics, Qingdao University, Qingdao 266071, China*

<sup>2</sup>*Department of Physics, Tsinghua University, Beijing 100084, China and*

<sup>3</sup>*State Key Laboratory of Magnetic Resonance and Atomic and Molecular Physics, Innovation Academy for Precision Measurement Science and Technology, Chinese Academy of Sciences, Wuhan 430071, China*

We theoretically calculate the density dynamic structure factor of one-dimensional Fermi superfluid with Raman-type spin-orbit coupling, and analyze its main dynamical character during phase transition between Bardeen-Cooper-Schrieffer superfluid and topological superfluid. Our theoretical results display four kinds of single-particle excitations induced by the two-branch structure of single-particle spectrum, and the cross single-particle excitation is much easier to be seen in the spin dynamic structure factor at a small transferred momentum. Also we find a new roton-like collective mode emerges at a fixed transferred momentum  $q \simeq 2k_F$ , and it only appears once the system enters the topological superfluid state. The occurrence of this roton-like excitation is related to switch of global minimum in single-particle spectrum from  $k = 0$  to  $k \simeq 2k_F$ .

## I. INTRODUCTION

Since the experimental realization of spin-orbit coupling (SOC) effect in ultracold atomic gases [1–3], it is possible to investigate many interesting and exotic matter states, like stripe phase [4] and topological state [5], etc, in this highly controllable system. To study properties of these many-body matter states, lots of scattering techniques based on the interplay between atoms and light play significant roles in enriching knowledge about them. For example, radio frequency can often be used to study the single-particle spectral function [6], while two-photon Bragg scattering technique is utilized to study both single-particle excitations and rich collective ones [7, 8].

As an many-body physical quantity, dynamic structure factor is related to the imaginary part of response function after Fourier transformation [10]. The definition of dynamic structure factor is related closely to a certain physical operator, which is applied to perturb system. Usually we focus our discussion on density operators of two spin components, which at the same time can impart a set of momentum and energy to the system to induce a density response. This density-related dynamic structure factor provides rich information about the dynamics of the system. At a small transferred momentum, the signal of dynamic structure factor is dominated by all possible collective excitations, like Goldstone phonon excitation [8], second sound [9], Leggett excitation [11–13], and possible Higgs excitation [14, 15]. At a large transferred momentum, the dynamic structure factor is mainly influenced by the single-particle excitation [16], which is determined by the many-body single-particle spectrum. Collecting all possible dynamical excitation displayed by dynamic structure factor, we

can effectively understand dynamical properties related to a certain many-body matter state of the system. Usually the experimental measurement of many-body physical quantities is a challenging work. However it is known that the density dynamic structure factor is proportional to the value of centre-of-mass velocity of the system [17], which makes it feasible to measure density structure factor by two-photon Bragg scattering experiment.

In this paper, we theoretically investigate one-dimensional (1D) Fermi superfluid with Raman-type SOC effect. The system can be realized by confining the motion of the system in other two dimension with optical lattice technique. This system has been found to experience a phase transition from a conventional Bardeen-Cooper-Schrieffer (BCS) superfluid to an interesting topological superfluid by continuously increasing an effective Zeeman field [5, 18, 19]. When the system comes into this topological superfluid, an impurity, a boundary or a topological defect can generate local Majorana fermions accompanied by a zero eigenenergy [21, 22, 28]. Since there is no symmetry breaking during phase transition, experimentally it is a great challenge to distinguish these two matter states. In this paper, we theoretically calculate the density dynamic structure factor of 1D Raman-SOC Fermi superfluid with random phase approximation [23], and analyze their main dynamical characters in both BCS and topological superfluid, which is expected to provide some dynamical information to understand and distinguish these two states.

This paper is organized as follows. In the next section, we will use the language of Green's function to introduce the microscopic model of 1D Fermi superfluid with Raman SOC effect, outline the mean-field approximation and how to calculate response function with random phase approximation. We give results of dynamic structure factor of both BCS and topological superfluid in Sec. III. In Sec. IV and V, we give our conclusions and acknowledgment. Some calculation details will be given in the final appendix.

\* hszhao@qdu.edu.cn

† pengshiguo@wipm.ac.cn

‡ phy.zoupeng@gmail.com

## II. METHODS

### A. Model and Hamiltonian

For a two spin-components 1D Raman-SOC Fermi superfluid with  $s$ -wave contact interaction, the system can be described by a model Hamiltonian

$$H = \sum_{\sigma} \int dx \psi_{\sigma}^{\dagger}(x) \left[ -\frac{1}{2m} \frac{\partial^2}{\partial x^2} - \mu \right] \psi_{\sigma}(x) - h \int dx \left[ \psi_{\uparrow}^{\dagger}(x) e^{i2k_R x} \psi_{\downarrow}(x) + H.c. \right] + g_{1D} \int dx \psi_{\uparrow}^{\dagger}(x) \psi_{\downarrow}^{\dagger}(x) \psi_{\downarrow}(x) \psi_{\uparrow}(x), \quad (1)$$

where  $\psi_{\sigma}(\psi_{\sigma}^{\dagger})$  is the annihilation (generation) operator of real particles with mass  $m$  for spin- $\sigma$  component and chemical potential  $\mu$ . A dimensionless parameter  $\gamma = mg_{1D}/n_0$  is usually used to describe the interaction strength  $g_{1D}$  of a uniform system at a bulk density  $n_0$ , by which we can define the Fermi wave vector  $k_F = \pi n_0/2$  and Fermi energy  $E_F = k_F^2/2m$ .  $h$  is an effective Zeeman field and  $k_R$  is the recoil momentum of SOC laser beam, both of which coming from the SOC effect. Here and in the following, we have set  $\hbar = k_B = 1$  for simple. In many related references about SOC effect, a further unitary transformation will be carried out to the above Hamiltonian [28], which induces a term  $\hat{k} \cdot \sigma$  turns out in the single-particle Hamiltonian ( $\sigma$  is Pauli matrix), and the same operation also changes the physical meaning of spin index. So here we do not carry out these transformation to keep the original definition of spin index.

A standard mean-field treatment is done to the interaction Hamiltonian  $H_{\text{int}} = g_{1D} \int dx \psi_{\uparrow}^{\dagger} \psi_{\downarrow}^{\dagger} \psi_{\downarrow} \psi_{\uparrow}$  with the usual definition of order parameter  $\Delta = -g_{1D} \langle \psi_{\downarrow} \psi_{\uparrow} \rangle$ . After Fourier transformation to the mean-field Hamiltonian, we can obtain its expression in the momentum representation, which reads

$$H_{\text{mf}} = \sum_{k\sigma} \xi_k c_{k\sigma}^{\dagger} c_{k\sigma} - h \left( c_{k+k_R\uparrow}^{\dagger} c_{k-k_R\downarrow} + H.c. \right) - \sum_k \left[ \Delta c_{k\uparrow}^{\dagger} c_{-k\downarrow}^{\dagger} + \Delta^* c_{-k\downarrow} c_{k\uparrow} \right] \quad (2)$$

with  $\xi_k = k^2/2m - \mu$ . Usually the order parameter  $\Delta$  is a complex number. However  $U(1)$  symmetry is broken in the ground state of the system, and the phase of  $\Delta$  is pushed to randomly choose an constant number. Here we can just take this phase to be zero, and induce  $\Delta = \Delta^*$ .

The exact diagonalization of mean-field Hamiltonian  $H_{\text{mf}}$  is a feasible but tedious work because of the long expression of each eigenvector. Luckily this embarrassing problem can be solved by motion equation of Green's function  $\omega \langle \langle c_1 | c_2 \rangle \rangle = \langle [c_1, c_2]_+ \rangle + \langle \langle c_1, H_{\text{mf}} | c_2 \rangle \rangle$ , where  $c_1$  and  $c_2$  are any possible fermionic operators of the system. Finally we find that the system has six independent Green's functions, which are

$$\begin{aligned} G_1(k, \omega) &\equiv \langle \langle c_{k+k_R\uparrow} | c_{k+k_R\uparrow}^{\dagger} \rangle \rangle = \sum_l [G_1]_k^l / (\omega - E_k^l), \\ G_2(k, \omega) &\equiv \langle \langle c_{k-k_R\downarrow} | c_{k-k_R\downarrow}^{\dagger} \rangle \rangle = \sum_l [G_2]_k^l / (\omega - E_k^l), \\ \Gamma(k, \omega) &\equiv \langle \langle c_{k+k_R\uparrow} | c_{-k-k_R\downarrow} \rangle \rangle = \sum_l [\Gamma]_k^l / (\omega - E_k^l), \\ S(k, \omega) &\equiv \langle \langle c_{k-k_R\downarrow} | c_{k+k_R\uparrow}^{\dagger} \rangle \rangle = \sum_l [S]_k^l / (\omega - E_k^l), \\ F_1(k, \omega) &\equiv \langle \langle c_{k+k_R\uparrow} | c_{-k+k_R\uparrow} \rangle \rangle = \sum_l [F_1]_k^l / (\omega - E_k^l), \\ F_2(k, \omega) &\equiv \langle \langle c_{k-k_R\downarrow} | c_{-k-k_R\downarrow} \rangle \rangle = \sum_l [F_2]_k^l / (\omega - E_k^l), \end{aligned} \quad (3)$$

where  $l = \pm 1, \pm 2$  denotes respectively all four quasi-particle energy spectrum  $E_k^{(+1)} = -E_k^{(-1)} = U_k$  and  $E_k^{(+2)} = -E_k^{(-2)} = D_k$ . Symbols  $U_k$  and  $D_k$  are the up and down-branch quasi-particle spectra, respectively,

$$U_k = \sqrt{E_k^2 + h^2 + k^2 \lambda^2 + 2\sqrt{E_k^2 h^2 + \tilde{\xi}_k^2 k^2 \lambda^2}}, \quad (4)$$

$$D_k = \sqrt{E_k^2 + h^2 + k^2 \lambda^2 - 2\sqrt{E_k^2 h^2 + \tilde{\xi}_k^2 k^2 \lambda^2}}, \quad (5)$$

with  $\tilde{\xi}_k = \xi_k + E_R$ ,  $\lambda = k_R/m$ ,  $E_R = k_R^2/2m$  and  $E_k = \sqrt{\tilde{\xi}_k^2 + \Delta^2}$ . These single-particle spectra do great influence to the static and dynamical properties of ground state. All expressions of  $[G_1]_k^l, [G_2]_k^l, [\Gamma]_k^l, [S]_k^l, [F_1]_k^l$  and  $[F_2]_k^l$  will be listed in the appendix. Based on the fluctuation and dissipation theorem, it is easy to get the relation between all physical quantities and corresponding Green's functions. For example, we obtain equations of density equation

$$n_1 = \sum_k \langle \langle c_{k\uparrow}^{\dagger} c_{k\uparrow} \rangle \rangle = -\frac{1}{\pi} \sum_k \int d\omega \frac{\text{Im} [G_1(k, \omega)]}{e^{\omega/T} + 1}, \quad (6)$$

$$n_2 = \sum_k \langle \langle c_{k\downarrow}^{\dagger} c_{k\downarrow} \rangle \rangle = -\frac{1}{\pi} \sum_k \int d\omega \frac{\text{Im} [G_2(k, \omega)]}{e^{\omega/T} + 1}, \quad (7)$$

and order parameter equation

$$\frac{\Delta}{g_{1D}} = -\sum_k \langle \langle c_{-k\downarrow} c_{k\uparrow} \rangle \rangle = \frac{1}{\pi} \sum_k \int d\omega \frac{\text{Im} [\Gamma(k, \omega)]}{e^{\omega/T} + 1}, \quad (8)$$

with Green's function  $G_1, G_2$  and  $\Gamma$  in Eq. 3 at temperature  $T$ . By self-consistently solving the above density and order parameter equations, the value of chemical potential  $\mu$  and order parameter  $\Delta$  can be numerically calculated.

In the following, we take an interaction strength  $\gamma = \pi$  and a typical experimental value of  $k_R = 0.75k_F$ . As

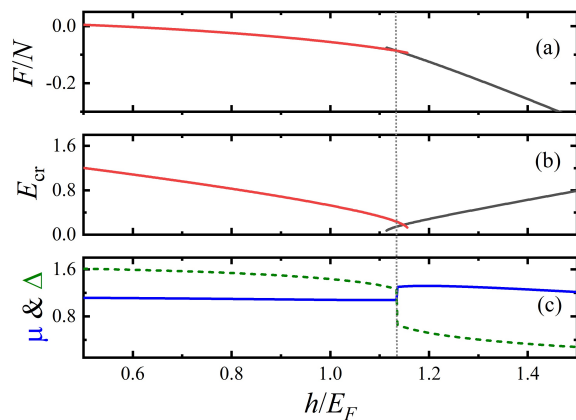


Figure 1. The distribution of Free energy in Panel (a),  $E_{\text{cr}} = \left| h - \sqrt{(\mu - E_R)^2 + \Delta^2} \right|$  in Panel (b), and chemical potential (blue solid line) and order parameter (olive dashed line) at different effective Zeeman field  $h$  during the phase transition between BCS superfluid (red solid line) and topological superfluid (black solid line). A gray dotted line marks the location of critical value of effective Zeeman magnetic field  $h_c = 1.135E_F$  at  $\gamma = \pi$  and  $k_R = 0.75k_F$ .

shown in Fig. 1, the system experiences a phase transition from BCS superfluid to topological superfluid when increasing continuously the effective Zeeman field  $h$  over a critical value  $h_c = 1.135E_F$ , in which the free energies of two states are equal with each other (see panel (a)). This is a first order phase transition, during which these two states compete with each other and make chemical potential  $\mu$  and order parameter  $\Delta$  experience a discontinuous variation at  $h_c$  (see panel (c)). It should be noticed that the critical Zeeman field  $h_c$  here is larger than the another critical value of Zeeman field  $h$  at which the topological superfluid just turn out and  $E_{\text{cr}} = \left| h - \sqrt{(\mu - E_R)^2 + \Delta^2} \right|$  just touches zero (see panel (b)).

The physical origin of this phase transition can also be understood from the geometrical structure of the down-branch single-particle spectrum  $D_k$ . As shown in Fig. 2, the global minimum of  $D_k$  experiences a switch from  $k = 0$  (red dotted line) to a non-zero  $k$  (black solid line), when continuously increasing Zeeman field  $h$ . In the critical point ( $h_c = 1.135E_F$ ), there are two options of matter state for atoms to stay in the momentum space, in which the value of chemical potential (Panel (c) of Fig. 1) can push all atoms to stay in the regime around  $k = 0$ , or both  $k = 0$  and non-zero  $k$  minimum. The competition between these two situations generate both BCS and topological superfluid with the same Free energy, and finally make the system experience this phase transition.

Next we will discuss the dynamical properties of the system and numerical methods to calculate them.

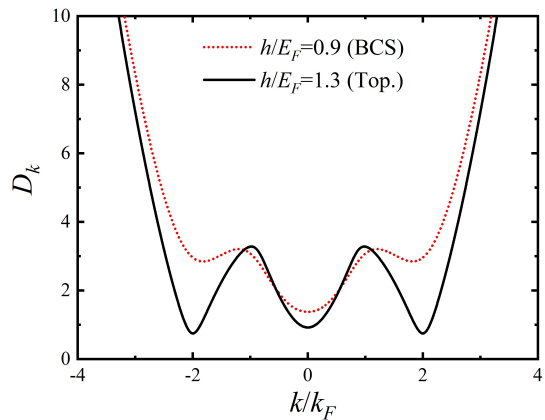


Figure 2. The distribution of down-branch single-particle spectrum  $D_k$  at  $\gamma = \pi$  and  $k_R = 0.75k_F$ .

## B. Response function and random phase approximation

In the Fermi superfluid, there are four different densities, which are denoted respectively by  $n_1 = \sum_k \langle c_{k\uparrow}^\dagger c_{k\uparrow} \rangle$ ,  $n_2 = \sum_k \langle c_{-k\downarrow}^\dagger c_{-k\downarrow} \rangle$ ,  $n_3 = \sum_k \langle c_{-k\downarrow} c_{k\uparrow} \rangle$  and  $n_4 = \sum_k \langle c_{k\uparrow}^\dagger c_{-k\downarrow}^\dagger \rangle$ . Due to the interaction between particles, these densities are closely coupled with each other. Any fluctuation in each kind of density will make the other densities generate an obvious density fluctuation of them. This physics plays a significant role in the dynamical excitation of the system, and also demonstrates the importance and necessity of the term in Hamiltonian beyond mean-field theory. Random phase approximation has been verified to be a feasible way to treat the fluctuation term of Hamiltonian [23]. Comparing with experiments, it can even obtain some quantitatively reliable predictions in three-dimensional Fermi superfluid [24, 25]. Its prediction also qualitatively agrees with quantum Monte Carlo data in two-dimensional Fermi system [15]. Here we also use the same method to carry out calculation, to qualitatively study the dynamical excitation of 1D SOC Fermi superfluid. Its main idea is introduced in the following.

Following the standard linear response theorem, a weak external density perturbations potential  $V_{\text{ext}} = [V_1, V_2, V_3, V_4]$ , which carries a specific momentum  $q$ , is exerted to the Fermi superfluid. The corresponding perturbation Hamiltonian is described by  $H_{\text{ext}} = \sum_{kq} \Psi_{k+q}^\dagger (V_1\sigma_1 + V_2\sigma_2 + V_3\sigma_3 + V_4\sigma_4) \Psi_k$ . Here  $\Psi_k = [c_{k\uparrow}, c_{-k\downarrow}^\dagger]^T$  is the field operator matrix in the momentum representation. Four matrices  $\sigma_1 = (I + \sigma_z)/2$ ,  $\sigma_2 = (I - \sigma_z)/2$ ,  $\sigma_3 = (\sigma_x - i\sigma_y)/2$ , and  $\sigma_4 = (\sigma_x + i\sigma_y)/2$  are defined with Pauli matrices  $\sigma_{x,y,z}$  and unit matrix  $I$ . This perturbation Hamiltonian  $H_{\text{ext}}$  will induce a density fluctuation of all densities, labeled by a

matrix

$$\rho_q = \sum_k \begin{bmatrix} n_{kq}^1 \\ n_{kq}^2 \\ n_{kq}^3 \\ n_{kq}^4 \end{bmatrix} = \sum_k \begin{bmatrix} \Psi_k^\dagger \sigma_1 \Psi_{k+q} \\ \Psi_k^\dagger \sigma_2 \Psi_{k+q} \\ \Psi_k^\dagger \sigma_3 \Psi_{k+q} \\ \Psi_k^\dagger \sigma_4 \Psi_{k+q} \end{bmatrix}. \quad (9)$$

These density fluctuation in reverse play a non-negligible role in generating a fluctuation Hamiltonian  $H_{sf} = \sum_q \rho_q^\dagger A_q$ , which is usually called self-consistent dynamical potential [26]. Here

$$A_q = \begin{bmatrix} n_q^2 \\ n_q^1 \\ n_q^3 \\ n_q^4 \end{bmatrix} = g_{1D} \sum_k \begin{bmatrix} n_{kq}^2 \\ n_{kq}^1 \\ n_{kq}^3 \\ n_{kq}^4 \end{bmatrix}$$

is the strength of fluctuation potential. Different from two or three dimension case, the contribution from  $n_q^3$  and  $n_q^4$  can is not divergent and there is no need to carry on renormalization to one dimension interaction strength  $g_{1D}$ .

In a weak perturbation situation, the amplitude of density fluctuation  $\rho_q$  is proportional to the external potential  $V_{ext}$ , and they are connected to each other by

$$\rho_q = \chi V_{ext}, \quad (10)$$

where  $\chi$  is the response function of the system and includes rich information about the dynamical excitation, however whose calculation is usually quite hard to be carried out. As discussed above, a feasible way to figure out this problem is to use random phase approximation, which collect effects of both  $V_{ext}$  and  $V_{sf} = M_I A_q$  to define an effective external potential

$$V_{eff} = V_{ext} + V_{sf}. \quad (11)$$

Then the motion of real gases in external potential  $V_{ext}$  is equivalent to the motion of mean-field gases in this effective potential  $V_{eff}$ . So the density fluctuation is connected to this effective potential  $V_{eff}$  by

$$\rho_q = \chi^0 V_{eff}, \quad (12)$$

where  $\chi^0$  is the response function in the mean-field approximation, whose calculation is relatively much easier. Finally, with Eqs. 9, 10,11, and 12, we find  $\chi$  and  $\chi^0$  is related to each other by equation

$$\chi = \frac{\chi^0}{1 - \chi^0 M_I g}, \quad (13)$$

where

$$M_I = \begin{bmatrix} 0 & 1 & 0 & 0 \\ 1 & 0 & 0 & 0 \\ 0 & 0 & 0 & 1 \\ 0 & 0 & 1 & 0 \end{bmatrix}$$

is a constant matrix reflecting the coupling situation of four different densities.

Next we discuss the derivation of the mean-field response function  $\chi^0$ , which is a  $4 \times 4$  matrix

$$\chi^0 = \begin{bmatrix} \chi_{11}^0 & \chi_{12}^0 & \chi_{13}^0 & \chi_{14}^0 \\ \chi_{21}^0 & \chi_{22}^0 & \chi_{23}^0 & \chi_{24}^0 \\ \chi_{31}^0 & \chi_{32}^0 & \chi_{33}^0 & \chi_{34}^0 \\ \chi_{41}^0 & \chi_{42}^0 & \chi_{43}^0 & \chi_{44}^0 \end{bmatrix}. \quad (14)$$

Here any matrix element  $\chi_{ij}^0(x_1, x_2, \tau, 0) \equiv -\langle \hat{n}_i(x_1, \tau) \hat{n}_j(x_2, 0) \rangle$ . In the uniform system, all response function should only be the function of relative coordinate  $x = x_1 - x_2$  and imaginary time  $\tau$ . So a generalized coordinate  $R = (x, \tau)$  is used to go on discussing. Based on Wick's theorem, we should consider all possible two-operators contraction terms, which are all related to 6 independent Green's functions in Eqs. 3. We find that the mean-field response function can be displayed by  $\chi^0 = A + B$ , in which  $A$  is the mean-field response function connecting to Green's functions  $G_1$ ,  $G_2$  and  $\Gamma$ , while  $B$  connecting the SOC Green's functions  $S$ ,  $F_1$  and  $F_2$ . For example, in the spatial and time representation,

$$\chi_{11}^0(R) \equiv -\langle \hat{n}_1(x_1, \tau) \hat{n}_1(x_2, 0) \rangle = A_{11}(R) + B_{11}(R)$$

where  $A_{11}(R) = G_1(-R)G_1(R)$  and  $B_{11}(R) = F_1^\dagger(-R)F_1(R)$ . In the ground state ( $\Delta = \Delta^*$ ), we find  $F_1^\dagger = F_1$ . After Fourier transformation to Green's functions and with identical relation  $\frac{1}{\beta} \sum_{ip_n} \frac{1}{ip_n - \varepsilon} * \frac{1}{ip_n + iq_n - \varepsilon'} = \frac{f(\varepsilon) - f(\varepsilon')}{iq_n + \varepsilon - \varepsilon'}$  ( $ip_n$  and  $iq_n$  are Matsubara frequencies, and  $f(x)$  is the Fermi distribution function), we obtain the expression of all matrix elements in the momentum-energy representation

$$\chi^0(q, \omega) = A(q, \omega) + B(q, \omega), \quad (15)$$

where

$$A = \begin{bmatrix} A_{11}, & A_{12}, & A_{13}, & A_{14} \\ A_{12}, & A_{22}, & A_{23}, & A_{24} \\ A_{14}, & A_{24}, & -A_{12}, & A_{34} \\ A_{13}, & A_{23}, & A_{43}, & -A_{12} \end{bmatrix}$$

has 9 independent matrix elements, and

$$B = \begin{bmatrix} B_{11}, & B_{12}, & B_{13}, & B_{14} \\ B_{12}, & B_{22}, & B_{23}, & B_{24} \\ B_{14}, & B_{24}, & B_{33}, & B_{34} \\ B_{13}, & B_{23}, & B_{43}, & B_{33} \end{bmatrix}$$

has 10 independent matrix elements. All expressions of these matrix elements are listed in the appendix.

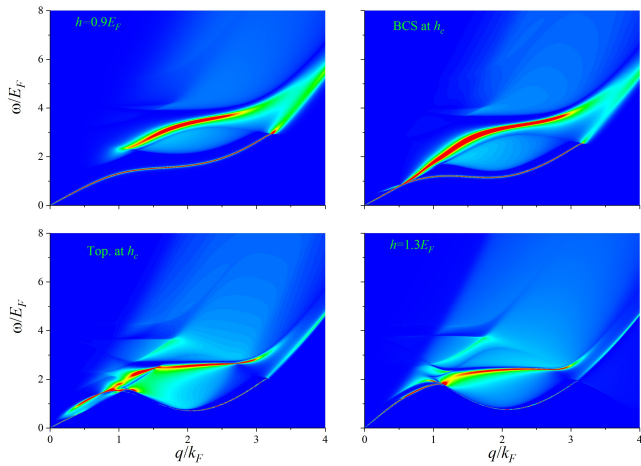


Figure 3. The density dynamic structure factor  $S_n(q, \omega)$  at different Zeeman field  $h = 0.9E_F, h_c, 1.3E_F$ .

### C. Dynamic structure factor

With Eqs. 13 and 15, we get expressions of both the density and spin response function, which are expressed by

$$\begin{aligned}\chi_n &\equiv \chi_{11} + \chi_{22} + \chi_{12} + \chi_{21}, \\ \chi_s &\equiv \chi_{11} + \chi_{22} - \chi_{12} - \chi_{21}.\end{aligned}\quad (16)$$

And the density dynamic structure factor  $S_n(q, \omega)$  and the spin one  $S_s(q, \omega)$  are connected with its corresponding response function by

$$S_{n/s} = -\frac{1}{\pi} \frac{1}{1 - e^{-\omega/T}} \text{Im} [\chi_{n/s}], \quad (17)$$

where  $q$  and  $\omega$  are the transferred momentum and energy, respectively. The sum rules of these two dynamic structure factors have been introduced in the reference [29].

## III. RESULTS

In the following discussions, we still focus on the interaction strength  $\gamma = \pi$  and also the recoil momentum  $k_R = 0.75k_F$  at zero temperature. These parameters are the same as one in Fig. 1. We numerically calculate the density and spin dynamic structure factor, which are shown in Fig. 3 and Fig. 4, respectively, in the phase transition between BCS superfluid (higher two panels) and topological superfluid (lower two panels). Generally we investigate a full dynamical excitation in different transferred momentum  $q$ , including the low energy (or momentum) collective excitation to the high energy (or momentum) single-particle excitation. Of course, the presence of SOC effect goes on enriching dynamical behaviors than the one in conventional Fermi superfluid.

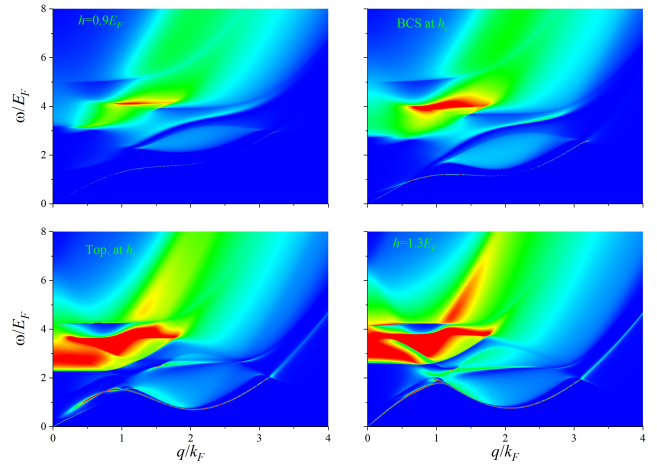


Figure 4. The spin dynamic structure factor  $S_s(q, \omega)$  at different Zeeman field  $h = 0.9E_F, h_c, 1.3E_F$ .

### A. Collective phonon and roton-like excitations

At a low transferred energy  $\omega$ , it is easy to investigate the collective excitation. By continuously increasing transferred momentum  $q$  from zero, we initially see a gapless phonon excitation in the density dynamic structure factor  $S_n(q, \omega)$ , which is shown by the lower red curve in all four panels of Fig. 3. When the system is in the BCS superfluid ( $h \leq h_c$ , higher two panels), the spectrum of collective phonon excitation just monotonically rises with transferred momentum  $q$ , and finally merges into the single-particle excitation continuum in a certain large enough  $q$ . In the whole BCS regime, the phonon velocity almost does not vary too much with the effective Zeeman field  $h$ , except a narrow regime close to transition where BCS superfluid becomes a metastable state and the velocity suddenly drops (red solid and dot line of Fig. 5). Of course, the gapless phonon excitation can also be seen in the topological superfluid (black solid and dot line of Fig. 5), and its velocity monotonically increases with Zeeman field  $h$  and finally saturates to a constant value. In the critical regime  $h = h_c$ , the BCS and topological state have the same Free energy. Although we calculate respectively their dynamic structure factor, the phonon excitation of one state may be potentially influenced by the other, and turns out a complex excitation behavior (see Fig. 3 and 4).

Besides the phonon collective excitation, we investigate a new collective roton-like excitation only appearing in the topological superfluid. As shown in the lower two panels of both Fig. 3 and 4, this roton-like excitation is a natural extension of the phonon mode, and it is denoted by a local minimum of the excitation spectrum at a fixed momentum  $q \simeq 2k_F$ , which is just the global minimum of the down-branch spectrum  $D_k$  (see red line of Fig. 2). There is no roton-like excitation in the BCS superfluid, where  $q \simeq 2k_F$  is just a local minimum and the

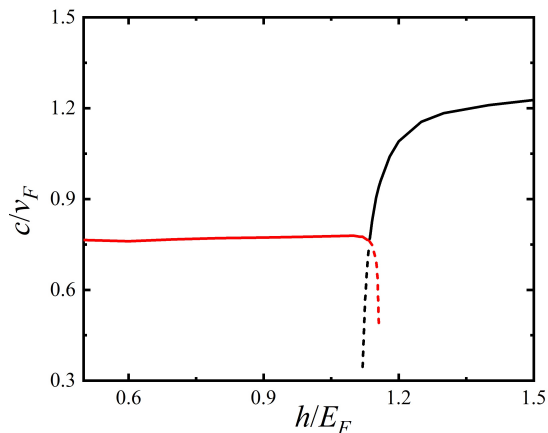


Figure 5. The sound velocity  $c$  at different effective Zeeman field  $h$ .

global minimum is located at  $q = 0$ . These results tell us that the emergence of roton-like excitation is closely related to the formation of global minimum at  $q \simeq 2k_F$ , which is just the character of spectrum  $D_k$  in topological superfluid. All discussions above hint that the specific single-particle effect brought by the SOC effect plays an important role in the appearance of the roton-like excitation at a certain interaction strength. For general, we have also checked that the same roton-like mode can be seen in other different interaction strength (for example  $\gamma = 2.5, 4.0$ ) and recoil momentum  $k_R$ , and the location of the roton-like excitation is always fixed at  $q \simeq 2k_F$ .

The dynamical behavior of collective mode can be displayed by both the density and spin dynamic structure factor. However a different excitation related to single-particle excitation happens at a relatively large transferred energy  $\omega$  when  $q$  is small, whose physical origin will be introduced in the following.

## B. Threshold of single-particle excitation spectrum

When the transferred energy  $\omega$  is large enough, a pair-breaking of Cooper pairs will occur and make pairs be separated into free Fermi atoms. Indeed a great part of the dynamical excitation in Fig. 3 and 4 is dominated by this pair-breaking effect. In the density dynamic structure factor  $S_n$ , this effect usually is much obvious in a relatively large transferred momentum  $q > k_F$ , where the collective excitation are depressed very much. Different from the conventional Fermi superfluid, this single-particle excitation takes up a large regime in the spin dynamic structure factor  $S_s$ , even for a small and zero transferred momentum  $q$ . Before understanding this single-particle excitation, it is necessary to study the threshold energy to break a Cooper pair.

This pair-breaking excitation is related to two-branch structure of quasi-particle spectrum  $U_k$  and  $D_k$ , and the two atoms forming a Cooper-pair can come from

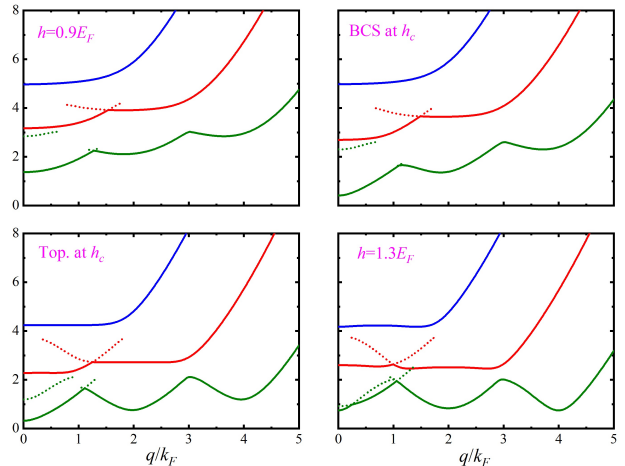


Figure 6. Four kinds of single-particle excitation spectra. Olive line:  $D_k \leftrightarrow D_{k+q}$ . Red line:  $D_k \leftrightarrow U_{k+q}$  and  $U_k \leftrightarrow D_{k+q}$ . Blue line:  $U_k \leftrightarrow U_{k+q}$ .

the same or different single-particle spectrum. This two-branch structure of spectrum generates much richer single-particle excitation than the conventional Fermi superfluid, and induces four possible combinations of Fermi atoms in a Cooper pair, namely the  $DD$ ,  $DU$ ,  $UD$ , and  $UU$  type. The minimum energy at a certain momentum  $q$  to break a pair should be  $\min[D_k + D_{k+q}]$ ,  $\min[D_k + U_{k+q}]$ ,  $\min[U_k + D_{k+q}]$  or  $\min[U_k + U_{k+q}]$ . Also due to the potential three wells geometry of down-branch spectrum  $D_k$ , there are not only the global minimum energy but also many possible local minima to break a Cooper pair in single-particle excitations. These results are shown in Fig. 6. The lowest olive line denote the  $DD$  excitation, and its minimum value of pair-breaking excitation is from the down-branch quasi-particle spectrum ( $\min[D_k + D_{k+q}]$ ). Besides global minimum, it also has two and even three local minima at some specific transferred momentum  $q$ , displayed by olive dotted lines. In other different regime of  $q$ , these local minima will disappear since the geometry of spectrum has been changed. From the BCS superfluid ( $h = 0.9E_F$ ) to the topological superfluid ( $h = 1.3E_F$ ), the value of order parameter  $\Delta$  monotonically decreases with effective Zeeman field  $h$  (shown by panel (b) of Fig.1). This behaviour make the pair-breaking excitation be much easier in a large  $h$ , and generally make olive line become lower and lower.

The red line denotes  $DU$  and  $UD$  excitations, which are overlapped with each other. The two atoms in a pair comes from different branch of spectrum. It starts from the  $\min[D_k + U_{k+q}]$ , whose energy is higher than the  $DD$  one. Similar to  $DD$  excitation, there are some possible local minima in these cross excitations. It should be emphasized that this  $DU$  single-particle excitation at a small  $q$  displays a much stronger excitation strength in the spin dynamic structure factor than one in density dynamic structure factor (see Fig. 4), which also reflect

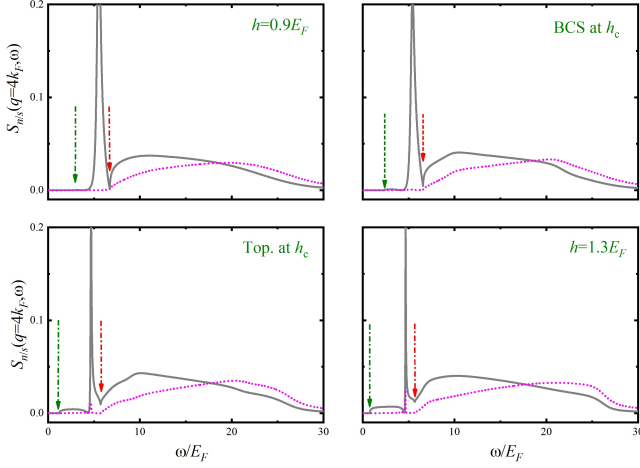


Figure 7. The density (gray) and spin (magenta) dynamical structure factor of 1D SOC Fermi superfluid at transferred momentum  $q = 4k_F$ .

the coupling between different spin components.

Starting from the  $\min[U_k + U_{k+q}]$ , the blue line is the  $UU$  excitation, which requires the largest excitation energy. This excitation has less density of state in the small  $q$  regime in the BCS superfluid, while topological state enhances its density of state and displays a relatively stronger signal.

All of these kinds of critical single-particle excitations are just located in the colorful edge curve of Fig.3 and Fig.4, and mark the regime of single-particle excitation. To better understand the dynamical excitation in these colorful panels, we will discuss the dynamic structure factor at a selected transferred momentum  $q$ .

### C. Dynamic excitation at a constant momentum $q$

For a relatively large transferred momentum  $q \gg k_F$ , the dynamic structure factor will be dominated by the single-particle excitation. As shown in Fig. 7, we investigate the density and spin dynamic structure factor at  $q = 4k_F$  in both BCS and topological superfluid. In all four panels, we can see two obvious single-particle excitations ( $DD$  and  $DU$  type) and a sharp collective phonon excitation. The locations of threshold energy for two single-particle excitations are respectively labeled by the olive and red dash-dot arrows. Here the phonon excitation has already been mixed with the  $DD$  single-particle excitation, which induces a non-zero expansion width to the peak of collective mode. Its location is between the olive and red arrows, after which more and more single-particle excitations turn out. There is no obvious  $UU$  excitation signal here, which is drowned into the background of other single-particle excitations. At  $q = 4k_F$ , it is easy to see that the topological superfluid displays a relatively stronger  $DD$  excitation  $q = 4k_F$  than one in BCS state.

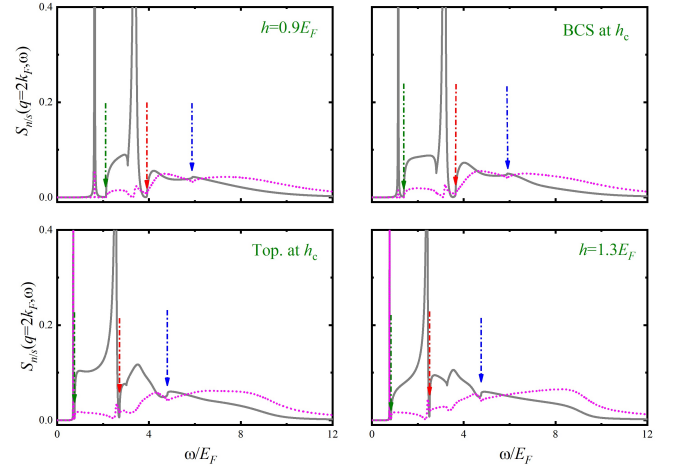


Figure 8. The density (gray) and spin (magenta) dynamical structure factor of 1D SOC Fermi superfluid at transferred momentum  $q = 2k_F$ .

When taking transferred momentum  $q = 2k_F$ , the competition between collective mode and single-particle mode is very intense. We watch a much richer dynamical excitation. As shown in Fig. 8, both  $S_n$  and  $S_s$  present two sharp delta-like peak and all three kinds of single-particle excitation, the threshold locations of which are still respectively labeled by olive, red and blue arrows. At  $q = 2k_F$ , the left sharp peak in four panels locates on the left side of green arrows ( $DD$  type excitation). In fact it is a natural extension of the collective phonon excitation, which is close to merge into the single-particle excitation continuum. The peak in topological superfluid (lower two panels) happens at a relative low excitation energy since the system generates a roton-like collective excitation, which has been discussed above. As to the right sharp peak, it locates at the higher red eyebrow position in Fig. 3, its physical origin is still an open question, we argue that it may be the possible collective Higgs oscillation, which has totally merged into the single-particle excitation [27].

For a much smaller transferred momentum  $q = 1k_F$ , the competition of all dynamical excitation displayed by two dynamic structure factors becomes much more intense, and the energy differences between all possible excitations are not far away from each other. The results of both BCS and topological state is shown in Fig. 9. When  $h = 0.9E_F$  (BCS), we see one clear phonon excitation around  $\omega \simeq 1.2E_F$ , and all other three kinds of single-particle excitations on its right hand, whose initial excitation energy are still marked by arrows. In this case,  $DU$  type excitation has two threshold energies. While the left red arrow is from the global minimum of excitation energy  $\min[D_k + U_{k+q}]$ , the right one comes from its local minimum. Similar physics also be found in  $h = h_c$  (BCS side). However a high peak ( $\omega \simeq 2.3E_F$ ) rises after olive arrows. When the system comes into the topologi-

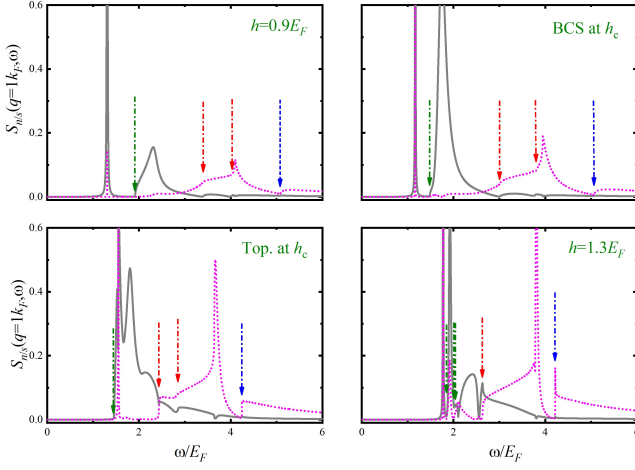


Figure 9. The density (blue) and spin (red) dynamical structure factor of 1D SOC Fermi superfluid at transferred momentum  $q = 1k_F$ .

cal regime ( $h = 1.3E_F$ ), this unknown peak ( $\omega \simeq 1.9E_F$ ) will present a delta-like excitation in a certain narrow energy regime (see also low-right panel of Fig. 3). It seems that this unknown peak is different from the unknown one discussed above. Maybe it is generated by the competition of two collective mode in two different states, and we argue it is the redundancy of collective mode in the metastable state. As to the single particle excitation, three minima of  $DD$  type have also been obtained in this case, and their positions are located by three olive arrows, each of which will induce the regular oscillation of the curve of dynamic structure factor.

#### IV. CONCLUSIONS AND OUTLOOK

In summary, we numerically calculate the density and spin dynamic structure factor of 1D Raman-SOC Fermi superfluid with random phase approximation during the phase transition between BCS and topological superfluid. The dynamic structure factor presents rich single-particle excitations and collective mode. Due to the two-branch structure of single-particle spectrum, there are three kinds of single-particle excitation, namely  $DD$ ,  $DU$  ( $UD$ ) and  $UU$  excitation. We also calculate their own threshold energy to break a Cooper pair. Among these single-particle excitation, the  $DU$  one takes a great part only in the spin dynamic structure factor at a small transferred momentum, which comes from the coupling effect between spin and orbital motion. As to collective excitation, these is an interesting roton-like collective excitation at  $k \simeq 2k_F$  when the system comes into the topological state. The generation of this roton-like excitation is due to the switch of global minimum of single-particle spectrum  $D_k$  from  $k = 0$  to  $k \simeq 2k_F$ . The similar physics has also been found in other different interaction strengths  $\gamma$

and recoil momenta  $k_R$ . Also these are some unknown quasi-delta like excitations when  $q$  is between  $k_F$  and  $2k_F$ , which are worth explaining its physical origin in our future research.

#### V. ACKNOWLEDGEMENTS

We are grateful for fruitful discussions with Hui Hu, Wei Yi and Wei Zhang. This research was supported by the National Natural Science Foundation of China, Grants No. 11804177 (P.Z.), No. 11547034 (H.Z.), No. 11974384 (S.-G.P.).

#### VI. APPENDIX

In this appendix, we will list expressions of 6 independent Green' functions and mean-field response function  $\chi^0 = A + B$ .

$$G_1(k, \omega) = \sum_l [G_1]_k^l / (\omega - E_k^l), \text{ with}$$

$$\begin{aligned} [G_1]_k^1 &= + \frac{U_k^2 - \xi_-^2 - h^2 - \Delta^2}{2(U_k^2 - D_k^2)} + \frac{\xi_+ U_k^2 - \xi_+ \xi_-^2 + \xi_- h^2 - \xi_+ \Delta^2}{2U_k(U_k^2 - D_k^2)}, \\ [G_1]_k^2 &= + \frac{U_k^2 - \xi_-^2 - h^2 - \Delta^2}{2(U_k^2 - D_k^2)} - \frac{\xi_+ U_k^2 - \xi_+ \xi_-^2 + \xi_- h^2 - \xi_+ \Delta^2}{2U_k(U_k^2 - D_k^2)}, \\ [G_1]_k^3 &= - \frac{D_k^2 - \xi_+^2 - h^2 - \Delta^2}{2(U_k^2 - D_k^2)} - \frac{\xi_+ D_k^2 - \xi_+ \xi_-^2 + \xi_- h^2 - \xi_+ \Delta^2}{2D_k(U_k^2 - D_k^2)}, \\ [G_1]_k^4 &= - \frac{D_k^2 - \xi_+^2 - h^2 - \Delta^2}{2(U_k^2 - D_k^2)} + \frac{\xi_+ D_k^2 - \xi_+ \xi_-^2 + \xi_- h^2 - \xi_+ \Delta^2}{2D_k(U_k^2 - D_k^2)}, \end{aligned}$$

where  $\xi_{\pm} = (k \pm k_R)^2 / 2m - \mu$ .  $G_2(k, \omega) = \sum_l [G_2]_k^l / (\omega - E_k^l)$ , with

$$\begin{aligned} [G_2]_k^1 &= + \frac{U_k^2 - \xi_+^2 - h^2 - \Delta^2}{2(U_k^2 - D_k^2)} + \frac{\xi_- U_k^2 - \xi_- \xi_+^2 + \xi_+ h^2 - \xi_- \Delta^2}{2U_k(U_k^2 - D_k^2)}, \\ [G_2]_k^2 &= + \frac{U_k^2 - \xi_+^2 - h^2 - \Delta^2}{2(U_k^2 - D_k^2)} - \frac{\xi_- U_k^2 - \xi_- \xi_+^2 + \xi_+ h^2 - \xi_- \Delta^2}{2U_k(U_k^2 - D_k^2)}, \\ [G_2]_k^3 &= - \frac{D_k^2 - \xi_-^2 - h^2 - \Delta^2}{2(U_k^2 - D_k^2)} - \frac{\xi_- D_k^2 - \xi_- \xi_+^2 + \xi_+ h^2 - \xi_- \Delta^2}{2D_k(U_k^2 - D_k^2)}, \\ [G_2]_k^4 &= - \frac{D_k^2 - \xi_-^2 - h^2 - \Delta^2}{2(U_k^2 - D_k^2)} + \frac{\xi_- D_k^2 - \xi_- \xi_+^2 + \xi_+ h^2 - \xi_- \Delta^2}{2D_k(U_k^2 - D_k^2)}. \end{aligned}$$

$\Gamma(k, \omega) = \sum_l [\Gamma]_k^l / (\omega - E_k^l)$ , with

$$\begin{aligned} [\Gamma]_k^1 &= - [\Gamma]_k^2 = - \frac{\Delta[U_k^2 - (\xi_-^2 - h^2 + \Delta^2)]}{2U_k(U_k^2 - D_k^2)}, \\ [\Gamma]_k^3 &= - [\Gamma]_k^4 = + \frac{\Delta[D_k^2 - (\xi_-^2 - h^2 + \Delta^2)]}{2D_k(U_k^2 - D_k^2)}. \end{aligned}$$

$S(k, \omega) = \sum_l [S]_k^l / (\omega - E_k^l)$ , with

$$\begin{aligned} [S]_k^1 &= h \left[ - \frac{\xi_+ + \xi_-}{2(U_k^2 - D_k^2)} - \frac{U_k^2 + \xi_+ \xi_- - h^2 + \Delta^2}{2U_k(U_k^2 - D_k^2)} \right], \\ [S]_k^2 &= h \left[ - \frac{\xi_+ + \xi_-}{2(U_k^2 - D_k^2)} + \frac{U_k^2 + \xi_+ \xi_- - h^2 + \Delta^2}{2U_k(U_k^2 - D_k^2)} \right], \\ [S]_k^3 &= h \left[ + \frac{\xi_+ + \xi_-}{2(U_k^2 - D_k^2)} + \frac{D_k^2 + \xi_+ \xi_- - h^2 + \Delta^2}{2D_k(U_k^2 - D_k^2)} \right], \\ [S]_k^4 &= h \left[ + \frac{\xi_+ + \xi_-}{2(U_k^2 - D_k^2)} - \frac{D_k^2 + \xi_+ \xi_- - h^2 + \Delta^2}{2D_k(U_k^2 - D_k^2)} \right]. \end{aligned}$$

$$F_1(k, \omega) = \sum_l [F_1]_k^l / (\omega - E_k^l), \text{ with}$$

$$\begin{aligned} [F_1]_k^1 &= -\frac{\Delta h(2U_k + \xi_+ - \xi_-)}{2U_k(U_k^2 - D_k^2)}, \\ [F_1]_k^2 &= -\frac{\Delta h(2U_k - \xi_+ + \xi_-)}{2U_k(U_k^2 - D_k^2)}, \\ [F_1]_k^3 &= +\frac{\Delta h(2D_k + \xi_+ - \xi_-)}{2D_k(U_k^2 - D_k^2)}, \\ [F_1]_k^4 &= +\frac{\Delta h(2D_k - \xi_+ + \xi_-)}{2D_k(U_k^2 - D_k^2)}. \end{aligned}$$

$$F_2(k, \omega) = \sum_l [F_2]_k^l / (\omega - E_k^l), \text{ with}$$

$$\begin{aligned} [F_2]_k^1 &= +\frac{\Delta h(2U_k - \xi_+ + \xi_-)}{2U_k(U_k^2 - D_k^2)}, \\ [F_2]_k^2 &= +\frac{\Delta h(2U_k + \xi_+ - \xi_-)}{2U_k(U_k^2 - D_k^2)}, \\ [F_2]_k^3 &= -\frac{\Delta h(2D_k - \xi_+ + \xi_-)}{2D_k(U_k^2 - D_k^2)}, \\ [F_2]_k^4 &= -\frac{\Delta h(2D_k + \xi_+ - \xi_-)}{2D_k(U_k^2 - D_k^2)}. \end{aligned}$$

The expressions of all 9 independent matrix elements in mean-field response function  $A$  are

$$\begin{aligned} A_{11} &= +\sum_{pll'} [G_1]_p^l [G_1]_{p+q}^{l'} \frac{f(E_p^l) - f(E_{p+q}^{l'})}{i\omega_n + E_p^l - E_{p+q}^{l'}}, \\ A_{12} &= -\sum_{pll'} [\Gamma]_p^l [\Gamma]_{p+q}^{l'} \frac{f(E_p^l) - f(E_{p+q}^{l'})}{i\omega_n + E_p^l - E_{p+q}^{l'}}, \\ A_{13} &= +\sum_{pll'} [G_1]_p^l [\Gamma]_{p+q}^{l'} \frac{f(E_p^l) - f(E_{p+q}^{l'})}{i\omega_n + E_p^l - E_{p+q}^{l'}}, \\ A_{14} &= +\sum_{pll'} [\Gamma]_p^l [G_1]_{p+q}^{l'} \frac{f(E_p^l) - f(E_{p+q}^{l'})}{i\omega_n + E_p^l - E_{p+q}^{l'}}, \\ A_{22} &= +\sum_{pll'} [G_2]_p^l [G_2]_{p+q}^{l'} \frac{f(E_p^l) - f(E_{p+q}^{l'})}{i\omega_n + E_p^l - E_{p+q}^{l'}}, \end{aligned}$$

$$\begin{aligned} A_{23} &= -\sum_{pll'} [\Gamma]_p^l [G_1]_{p+q}^{l'} \frac{f(E_p^l) - f(E_{p+q}^{l'})}{i\omega_n + E_p^l - E_{p+q}^{l'}}, \\ A_{24} &= -\sum_{pll'} [G_1]_p^{-l} [\Gamma]_{p+q}^{l'} \frac{f(E_p^l) - f(E_{p+q}^{l'})}{i\omega_n + E_p^l - E_{p+q}^{l'}}, \\ A_{34} &= +\sum_{pll'} [G_2]_p^{-l} [G_2]_{p+q}^{l'} \frac{f(E_p^l) - f(E_{p+q}^{l'})}{i\omega_n + E_p^l - E_{p+q}^{l'}}, \\ A_{43} &= +\sum_{pll'} [G_1]_p^l [G_1]_{p+q}^{-l'} \frac{f(E_p^l) - f(E_{p+q}^{l'})}{i\omega_n + E_p^l - E_{p+q}^{l'}}, \end{aligned}$$

where  $f(x) = 1/(e^{x/k_B T} + 1)$  is the Fermi-Dirac distribution function. The expressions of 10 independent matrix elements in mean-field response function  $B$  are

$$\begin{aligned} B_{11} &= -\sum_{pll'} [F_1]_p^l [F_1]_{p+q}^{l'} \frac{f(E_p^l) - f(E_{p+q}^{l'})}{i\omega_n + E_p^l - E_{p+q}^{l'}}, \\ B_{12} &= +\sum_{pll'} [S]_p^l [S]_{p+q}^{l'} \frac{f(E_p^l) - f(E_{p+q}^{l'})}{i\omega_n + E_p^l - E_{p+q}^{l'}}, \\ B_{13} &= -\sum_{pll'} [S]_p^l [F_1]_{p+q}^{l'} \frac{f(E_p^l) - f(E_{p+q}^{l'})}{i\omega_n + E_p^l - E_{p+q}^{l'}}, \\ B_{14} &= -\sum_{pll'} [F_1]_p^l [S]_{p+q}^{l'} \frac{f(E_p^l) - f(E_{p+q}^{l'})}{i\omega_n + E_p^l - E_{p+q}^{l'}}, \\ B_{22} &= -\sum_{pll'} [F_2]_p^l [F_2]_{p+q}^{l'} \frac{f(E_p^l) - f(E_{p+q}^{l'})}{i\omega_n + E_p^l - E_{p+q}^{l'}}, \\ B_{23} &= +\sum_{pll'} [S]_p^l [F_2]_{p+q}^{l'} \frac{f(E_p^l) - f(E_{p+q}^{l'})}{i\omega_n + E_p^l - E_{p+q}^{l'}}, \\ B_{24} &= +\sum_{pll'} [F_2]_p^l [S]_{p+q}^{l'} \frac{f(E_p^l) - f(E_{p+q}^{l'})}{i\omega_n + E_p^l - E_{p+q}^{l'}}, \\ B_{33} &= -\sum_{pll'} [F_2]_p^l [F_1]_{p+q}^{l'} \frac{f(E_p^l) - f(E_{p+q}^{l'})}{i\omega_n + E_p^l - E_{p+q}^{l'}}, \\ B_{34} &= -\sum_{pll'} [S]_p^{-l} [S]_{p+q}^{l'} \frac{f(E_p^l) - f(E_{p+q}^{l'})}{i\omega_n + E_p^l - E_{p+q}^{l'}}, \\ B_{43} &= -\sum_{pll'} [S]_p^l [S]_{p+q}^{-l'} \frac{f(E_p^l) - f(E_{p+q}^{l'})}{i\omega_n + E_p^l - E_{p+q}^{l'}}. \end{aligned}$$

- 
- [1] Y.-J. Lin, K. Jiménez-García & I. B. Spielman, *Spin-orbit-coupled Bose-Einstein condensates*, Nature **471**, 83–86 (2011).
- [2] P. Wang, Z.-Q. Yu, Z. Fu, J. Miao, L. Huang, S. Chai, H. Zhai, and J. Zhang, *Spin-Orbit Coupled Degenerate Fermi Gases*, Phys. Rev. Lett. **109**, 095301 (2012).
- [3] L. W. Cheuk, A. T. Sommer, Z. Hadzibabic, T. Yefsah, W. S. Bakr, and M. W. Zwierlein, *Spin-Injection Spectroscopy of a Spin-Orbit Coupled Fermi Gas*, Phys. Rev. Lett. **109**, 095302 (2012).
- [4] Tin-Lun Ho and Shizhong Zhang, *Bose-Einstein Condensates with Spin-Orbit Interaction*, Phys. Rev. Lett. **107**, 150403 (2011).
- [5] L. Jiang, T. Kitagawa, J. Alicea, A. R. Akhmerov, D. Pekker, G. Refael, J. Ignacio Cirac, E. Demler, M. D. Lukin, and P. Zoller, *Majorana Fermions in Equilibrium and in Driven Cold-Atom Quantum Wires*, Phys. Rev. Lett. **106**, 220402 (2011).
- [6] C. Chin and P. S. Julienne, *Radio-frequency transitions on weakly bound ultracold molecules*, Phys. Rev. A **71**, 012713 (2005).
- [7] G. Veeravalli, E. Kuhnle, P. Dyke, and C. J. Vale, *Bragg Spectroscopy of a Strongly Interacting Fermi Gas*, Phys. Rev. Lett. **101**, 250403 (2008).
- [8] S. Hoinka, P. Dyke, M. G. Lingham, J. J. Kinnunen, G. M. Bruun and C. J. Vale, Goldstone mode and pair-breaking excitations in atomic Fermi superfluid, Nat. Phys. **13**, pages943–946 (2017).
- [9] H. Hu, X.-C. Yao, and X.-J. Liu, *Second sound with ultracold atoms: A brief historical account*, arXiv:2206.05914v2.
- [10] L. Pitaevskii and S. Stringari, *Bose-Einstein Condensation*, (Oxford University Press, Oxford, 2003).
- [11] A. J. Leggett, *Number-phase fluctuations in two-band superconductors*, Prog. Theor. Phys. **36**, 901 (1966).
- [12] Y.-C. Zhang, S. Ding, and S. Zhang, *Collective modes in a twoband superfluid of ultracold alkaline-earth-metal atoms close to an orbital Feshbach resonance*, Phys. Rev. A **95**, 041603(R) (2017).
- [13] P. Zou, H. Zhao, L. He, X.-J. Liu, and H. Hu, *Dynamic structure factors of a strongly interacting Fermi superfluid near an orbital Feshbach resonance across the phase*

- transition from BCS to Sarma superfluid*, Phys. Rev. A **103**, 053310 (2021).
- [14] D. Pekker and C. Varma, *Amplitude/Higgs modes in condensed matter physics*, Annual Review of Condensed Matter Physics **6**, 269 (2015).
- [15] H. Zhao, X. Gao, W. Liang, P. Zou and F. Yuan, *Dynamical structure factors of a two-dimensional Fermi superfluid within random phase approximation*, New J. Phys. **22**, 093012 (2020).
- [16] R. Combescot, S. Giorgini and S. Stringari, *Molecular signatures in the structure factor of an interacting Fermi gas*, Europhys. Lett., **75** (5), pp. 695–701 (2006).
- [17] A. Brunello, F. Dalfovo, L. Pitaevskii, S. Stringari, and F. Zambelli, *Momentum transferred to a trapped Bose-Einstein condensate by stimulated light scattering*, Phys. Rev. A **64**, 063614 (2001).
- [18] X.-J. Liu and H. Hu, *Topological superfluid in one-dimensional spin-orbit-coupled atomic Fermi gases*, Phys. Rev. A **85**, 033622 (2012) .
- [19] R. Wei, and E. J. Mueller, *Majorana fermions in one-dimensional spin-orbit-coupled Fermi gases*, Phys. Rev. A **86**, 063604 (2012).
- [20] X.-J. Liu, *Impurity probe of topological superfluids in one-dimensional spin-orbit-coupled atomic Fermi gases*, Phys. Rev. A **87**, 013622 (2013).
- [21] ] Y. Xu, L. Mao, B. Wu, and C. Zhang, *Dark Solitons with Majorana Fermions in Spin-Orbit-Coupled Fermi Gases*, Phys. Rev. Lett. **113**, 130404 (2014).
- [22] X.-J. Liu, *Soliton-induced Majorana fermions in a one-dimensional atomic topological superfluid*, Phys. Rev. A **91**, 023610 (2015).
- [23] P. W. Anderson, *Random-Phase Approximation in the superconductivity*, Phys. Rev. **112**, 1900 (1958).
- [24] P. Zou, E. D. Kuhnle, C. J. Vale, and H. Hu, *Quantitative comparison between theoretical predictions and experimental results for Bragg spectroscopy of a strongly interacting Fermi superfluid*, Phys. Rev. A **82**, 061605(R) (2010).
- [25] P. Zou, H. Hu, and X.-J. Liu, *Low-momentum dynamic structure factor of a strongly interacting Fermi gas at finite temperature: The Goldstone phonon and its Landau damping*, Phys. Rev. A **98**, 011602(R) (2018).
- [26] X.-J. Liu, H. Hu, A. Minguzzi, and M. P. Tosi, *Collective oscillations of a confined Bose gas at finite temperature in the random-phase approximation*, Phys. Rev. A **69**, 043605 (2004) .
- [27] G. Fan, X.-L. Chen , and P. Zou, *Probing two Higgs oscillations in a one-dimensional Fermi superfluid with Raman-type spin-orbit coupling*, Front. Phys. **17**(5), 52502 (2022).
- [28] X.-J. Liu, *Impurity probe of topological superfluids in one-dimensional spin-orbit-coupled atomic Fermi gases*, Phys. Rev. A **87**, 013622 (2013).
- [29] L. He and Z.-Q. Yu, *Dynamic structure factors and sum rules in two-component quantum gases with spin-orbit coupling*, Acta Phys. Sin., **65**, 131101 (2016).